X-ray absorption spectroscopy study of local structural changes in a-WO_3 under colouration

1993 J. Phys.: Condens. Matter 5 2333

(http://iopscience.iop.org/0953-8984/5/15/006)

J. Phys.: Condens. Matter 5 (1993) 2333–2340. Printed in the UK

X-ray absorption spectroscopy study of local structural changes in a-WO_3 under colouration

A Kuzmin and J Purans
Institute of Solid State Physics, University of Latvia, Kengaraga 8, LV-1063 Riga, Latvia

Received 6 January 1993

Abstract. X-ray absorption spectroscopy has been applied to the study of local structural changes in amorphous tungsten trioxide thin films under colouration in an acid aqueous solution. It has been found that the formation of W^{5+} coloured centres is accompanied by the appearance of local deformations around them. It is shown that this effect can be associated with the formation of small-radius polarons.

1. Introduction

Amorphous tungsten trioxide (a-WO_3) thin films demand interest due to their electrochromic properties [1]. In recent years, they have been studied by different techniques [2–5], but the question about the correlation between their electrochromic properties and structure is still unsolved.

According to Faughnan and co-workers [6], the electrochromic effect can be interpreted as proton and electron injection in a-WO_3 with the formation of hydrogen tungsten bronze:

$$WO_3 + xH^+ + xe^- \rightarrow H_xWO_3. \tag{1}$$

Amorphous $W^{6+}O_3$ is transparent, while tungsten bronze H_xWO_3 containing W^{5+} species is absorbing and has a blue or deep blue colour. Other small cations, such as Li^+ and Na^+, can also play the role of hydrogen [1]. It is known from electron paramagnetic resonance [2] and x-ray photoelectron spectroscopy [5] that electrochromism is associated with tungsten ions in a 5+ valence state. The colouration of the electrochromic film can be explained by several models [6–9], two of which are more acceptable than the others [1]: (i) intervalence transitions between W^{5+} and W^{6+} sites [6] or (ii) polaron absorption [7]. In the first case, the electrons injected into WO_3 and trapped at tungsten sites lead only to changes in the electronic structure of tungsten ions and their role is to compensate the additional positive charge of the injected protons (H^+). In the second model, the electrons additionally perturb the surrounding lattice and cause local deformations around W^{5+}. Thus, to distinguish between these two models, it is necessary to determine the local structure around coloured centres, but up to now such information has remained unknown, and the general question about structural changes induced by the electron and cation accommodation remains open.

Our preliminary results [10] show that a small change in the average W–O distance in the first coordination shell of tungsten appears under colouration in a-WO_3 thin films with prominent electrochromic properties. We proposed that observed structural changes correspond to the formation of small-radius polarons. In this work we present an accurate x-ray absorption spectroscopy study of local structural changes around tungsten in a-WO_3 thin films under the colouration process, which confirms fully our previous suggestion.

0953-8984/93/152333+08$07.50

2. Experimental methods and data analysis

Amorphous tungsten trioxide (a-WO_3) thin films were prepared by thermal evaporation of WO_3 powder in a medium vacuum on a polyimide substrate at two different temperatures $T_s = 340$ and 390 K.

The x-ray absorption spectra (XAS) were measured in transmission mode at the ADONE storage ring (Frascati, Italy) using the EXAFS station on the PWA BX-1 wiggler beam line. The electron energies during two sets of measurements were 1.2 and 1.5 GeV, with current 20–40 mA. The synchrotron radiation was monochromatized using the Si(111) ($2d = 6.271$ Å) channel-cut crystal monochromator, and its intensity was measured by two ionization chambers filled with krypton gas. The experimental spectra were recorded in the energy range $\sim$ 1000 eV at the W L_3-edge ($E_{L_3} = 10206$ eV) with an energy resolution equal to $\sim$ 1 eV.

The measurements for each sample were done during one injection of the ADONE ring at room temperature before (transparent film) and immediately after colouration (deep-blue film) in an acid (H_2SO_4) aqueous solution by contacting with an indium wire [2]. The samples were prepared as a set of several thin films with the total thickness x to have the resulting absorption jump $\Delta\mu x \simeq 1.0$–1.5 (where μ is the absorption coefficient). The crystalline monoclinic tungsten trioxide (c-WO_3) was used as a reference compound [4].

The experimental data were analyzed by the EXAFS (extended x-ray absorption fine structure) data analysis software package EDA [11]. The x-ray absorption coefficient $\mu(E) = \ln(I_0/I)$ was calculated from the intensities of synchrotron radiation, measured by two ionization chambers, before (I_0) and after (I) the sample. The background contribution $\mu_b(E)$ was approximated by the Victoreen rule ($\mu_b = A/E^3 + B/E^4$) and subtracted from the experimental spectrum $\mu(E)$. The resulting absorption coefficient in the vicinity of the edge is shown for both transparent and coloured thin films in figure 1.

Furthermore, the atomic-like contribution $\mu_0(E)$ was found by a combined polynomial/cubic-spline technique to have a precise removal of the EXAFS signal zero-line, and the EXAFS signal $\chi(E)$ was determined as $\chi(E) = (\mu - \mu_b - \mu_0)/\mu_0$. To convert $\chi(E)$ into the space of the photoelectron wavevector k, defined as $k = \sqrt{(2m/\hbar^2)(E - E_0)}$ where $E - E_0$ is the photoelectron kinetic energy measured from the inner core photoemission threshold (vacuum level), the energy origin E_0 was located at $\sim$ 5 eV above the white-line maximum according to the method utilized by us earlier [12]. The EXAFS signal $\chi(k)$ was multiplied by a factor k^2 to compensate the decrease in its amplitude with the increase in the wavevector value (figure 2(*a*)).

Table 1. The local structure around tungsten in a-WO_3 and c-WO_3 by EXAFS and x-ray diffraction (XRD). N is the coordination number (±0.3), R is the distance between tungsten and oxygen (±0.02), and σ^2 is the Debye–Waller factor (±0.0005).

EXAFS									XRD	
W^{5+} in a-WO_3			W^{6+} in a-WO_3			W^{6+} in c-WO_3				
N	R (Å)	σ^2 (Å^2)	N	R (Å)	σ^2 (Å^2)	N	R (Å)	σ^2 (Å^2)	N	R (Å)
1.61	1.820	0.0005	1.62	1.741	0.0009	1.54	1.758	0.0005	1.0	1.74
1.40	1.956	0.0043	2.09	1.848	0.0026	1.41	1.839	0.0003	1.5	1.84
1.33	1.992	0.0064	1.05	1.960	0.0135	1.51	1.944	0.0165	1.5	1.90
1.66	2.188	0.0136	1.24	2.054	0.0147	1.55	2.154	0.0066	2.0	2.11

In addition, the Fourier transform (FT) with a Gaussian window of the EXAFS $\chi(k)k^2$

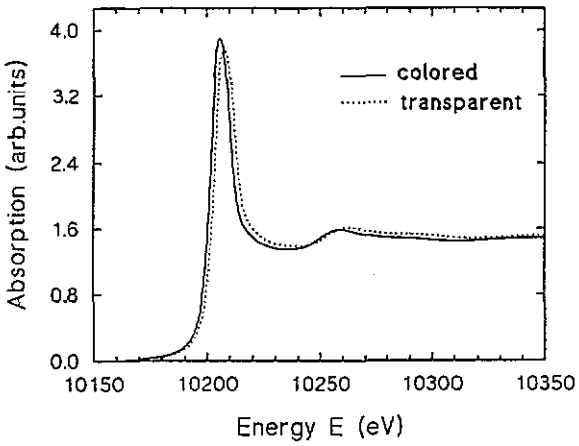

Figure 1. Experimental x-ray absorption spectra of the W L_3-edge in transparent (dotted curve) and coloured (full curve) a-WO_3 thin films. (Only the XANES region is shown.)

signal in the range 0.3–14.4 $Å^{-1}$ was calculated (figure 2(*b*)), and the contributions from the three clearly visible peaks were singled out by the back FT in the ranges 0.7–1.9 Å, 2.2–2.9 Å and 2.9–4.2 Å. They correspond to signals from the first shell, multiple-scattering in the first shell and the second shell (figure 3) [4]. The thus-obtained first-shell EXAFS $\chi(k)k^2$ signals in the range 3.0–13.0 $Å^{-1}$ were utilized in a best fit multishell analysis procedure with the backscattering amplitudes and phases, which were calculated using the FEFF3 code [13] and verified using the c-WO_3 reference compound. The results of the fitting procedure for c-WO_3 are presented in table 1, and they are in good agreement with the x-ray diffraction data [14]. The fitted parameters were coordination numbers, distances and Debye–Waller factors. The mean-free path contribution was included automatically in the scattering amplitude function by the use of the complex Hedin–Lundqvist exchange and correlation potential in the scattering T-matrix calculation [12, 13].

3. Results and discussion

3.1. XANES

The near-edge regions of the experimental x-ray absorption spectra at the W L_3-edge in a-WO_3 are shown in figure 1. The strong resonance near the absorption edge at $\sim$ 10205 eV is a so-called 'white line', and it is attributed to the $2p \rightarrow \overline{5, \epsilon}d$ transition. In this process the final state of the photoelectron is the state in the continuum (ϵ) with 5d atomic character. The bar over $\overline{5, \epsilon}d$ indicates that the photoelectron state is the relaxed excited state in the presence of the core hole at the 2p level screened by other electrons.

The difference between XAS for the transparent and coloured a-WO_3 thin films is already visible in a comparison of their x-ray absorption near-edge structures (XANES) (figure 1). For the coloured films (i) the position of the edge is shifted by about 1.5–1.8 eV to lower energies, and (ii) the amplitude of the 'white line' is a little bit higher.

The first effect was expected and can be easily understood by the smaller charge of the part of the absorbing tungsten atoms in the coloured film. The value of the shift depends

on many factors, such as the concentration of coloured centres, charge transfer effects, the symmetry of the absorbing centre and the distances between tungsten and oxygen in the first coordination shell. The calculation, done for the free tungsten ion in 6+ and 5+ states, shows that one could expect an energy difference for the 2p → 5d atomic transition of about 10 eV, which differs strongly from the observed value. It means that the influence of the bonding effect with oxygen ligands is high and the concentration of 5+ coloured centres is not dominant.

The second effect is within the error bar of the 'white line' amplitude measurements for several samples, and it will be verified more precisely in future planned experiments.

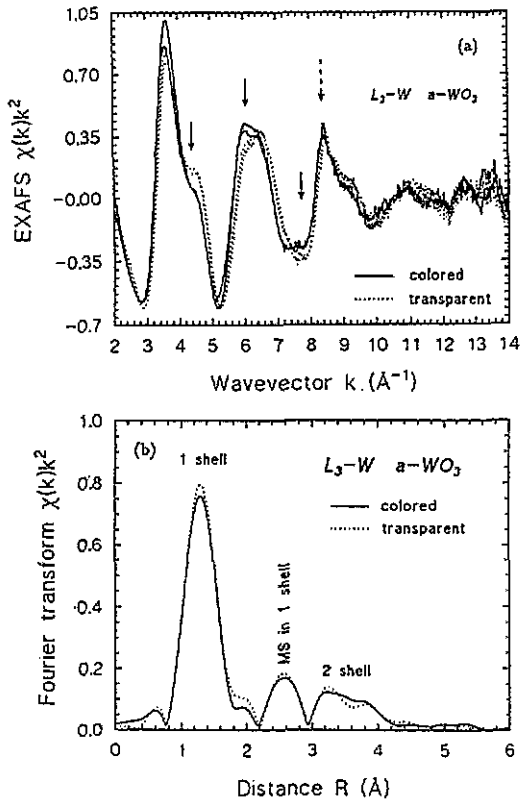

Figure 2. (*a*) Experimental EXAFS $\chi(k)k^2$ spectra of the W L_3-edge in a-WO_3 thin films for two samples before (dotted curve) and immediately after colouration (full curve). Two spectra for each case correspond to different samples. The full arrows indicate the main observed differences. The broken arrow marks the position of the double excitation 2p4d → 5d5d [15,16]. (*b*) Fourier transforms of the W L_3-edge EXAFS $\chi(k)k^2$. Dotted curve: transparent film; full curve: coloured film.

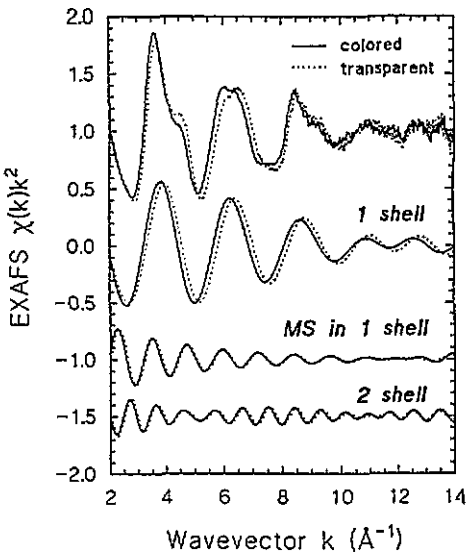

Figure 3. The separate contributions to the experimental signals (upper curves) from the scattering processes inside the first two shells. Dotted curve: transparent film; full curve: coloured film.

3.2. EXAFS

The experimental EXAFS $\chi(k)k^2$ signals and their Fourier transforms for transparent and coloured thin films are shown in figure 2. One can see a set of clearly visible differences

in the EXAFS signals, indicated by full arrows. Note that, in the EXAFS spectra at the W L_3-edge, the contribution from the multiple-electron excitation 2p4d → 5d5d was found recently [15, 16]. Its approximate position is shown in figure 2(*a*) by a broken arrow. The theoretical estimate of the contribution from such a multi-electron process is a few per cent from the amplitude of the 'white line' [16]. It is known [15] that it contributes as a step-like function resulting in additional noise or in an increase of the background over the whole range of the FT. In our case the noise component can be estimated from the level of the signal at large distances (greater than 4 Å) in FT (see figure 2(*b*)). From its small amplitude, we conclude that the distortion of the experimental spectrum due to the multiple-electron excitation is very small.

In FT of the EXAFS signals there are three clearly separated peaks, which can be attributed to single-scattering (SS) processes in the first coordination shell formed by oxygen (the peak at 0.7–1.9 Å), to the multiple-scattering (MS) contribution from the first shell (the peak at 2.2–2.9 Å) and to the complex contribution from the SS plus MS signals in the second shell formed by tungstens and distant oxygens (the peak at 2.9–4.2 Å). Note that the FTs have not been corrected on the photoelectron phase shift, therefore the positions of peaks in figure 2(*b*) differ from the true crystallographic values. To show which signal causes the difference between the EXAFS spectra from the transparent and coloured films, the back FTs in three ranges discussed above were calculated, and the result is shown in figure 3. One can see that the largest difference in the frequency of the EXAFS curves is observed in the first shell. Note that a higher frequency corresponds to a longer distance. Thus, we can already conclude from the comparative analysis of the experimental spectra that the colouration process leads to local structural changes, resulting mainly in an increase of the average tungsten–oxygen bond length. To understand how large the effect is, the qualitative analysis of the experimental signals from the first shell was done by the multishell best-fit procedure. Further, we will use the terms 'one-component', 'two-component' and 'multi-component' models to distinguish between the crystallographic coordination shells and the number of the individual EXAFS signals used in the fitting procedure to describe the experimental data.

At the beginning we fitted both signals using the one-component model to evaluate the average values of the parameters. It is possible to use such an approach because the shape of the experimental signal has not beat as for c-WO_3 [4]. The result is that both the average distance ($\langle R \rangle$) and the Debye–Waller factor ($\langle \sigma^2 \rangle$) values increase under colouration, and are equal to $\langle R \rangle = 1.767$ Å and $\langle \sigma^2 \rangle = 0.0038$ Å^2 for the transparent film, and $\langle R \rangle = 1.792$ Å and $\langle \sigma^2 \rangle = 0.0051$ Å^2 for the coloured film. Taking into account that only some of the tungsten ions transform into the W^{5+} state [5], we have evaluated the approximate ratio W^{5+}/W^{6+} from the ratio of the coordination numbers extracted from the two-component fitting procedure of the first-shell EXAFS signal for the coloured film. The obtained structural parameters of the two-component model are equal to $N = 1.40$, $R = 1.767$ Å, $\sigma^2 = 0.0021$ Å^2 and $N = 0.80$, $R = 1.881$ Å, $\sigma^2 = 0.0027$ Å^2, where the first set of data coincides well with the parameters of the one-component model for the transparent film and, thus, corresponds to W^{6+} sites. The second set is attributed to W^{5+} sites. Thus, the concentration of W^{5+} ions is about 36% and the electrochromic reaction in our case can be written in the form

$$W^{6+}O_3 + xH^+ + xe^- \rightarrow H_x(W^{5+}O_3)_x(W^{6+}O_3)_{1-x} \qquad x \approx 0.36. \tag{2}$$

We can now isolate the contribution from W^{5+} centres by subtracting from the total experimental EXAFS signal for the coloured film the total signal for the transparent film

multiplied by a factor 0.64 (figure 4(*a*)). Further, the contribution from the first shell around W^{5+} was extracted by the Fourier filtering procedure and used in the following analysis.

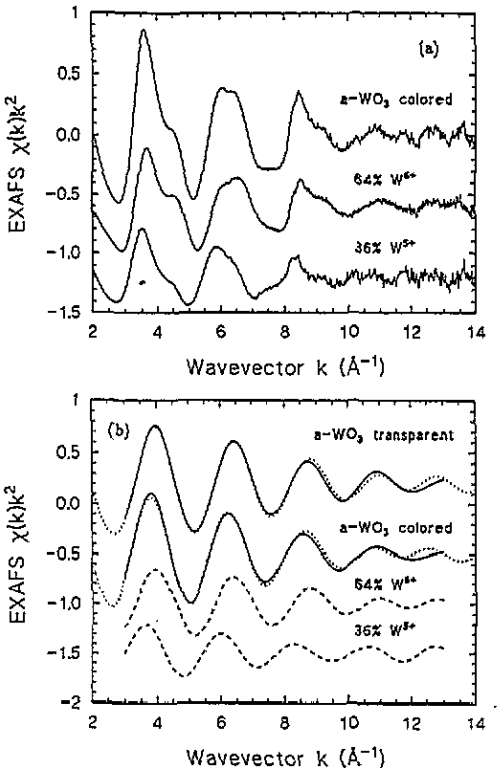

Figure 4. (*a*) Experimental EXAFS $\chi(k)k^2$ of the W L_3-edge in the coloured a-WO_3 thin film and its decomposition into two contributions from W^{6+} and W^{5+} sites. The ratio $\chi(W^{5+})/\chi(W^{6+})$ of two signals was estimated from the two-component best-fit procedure as discussed in the text. (*b*) Results of the four-component best-fit analysis for the transparent and coloured a-WO_3 thin films. Dotted curves: experiment; full curves: total calculated signals; broken curves: calculated contributions to the total signal from sites with a different valence state of tungsten ions.

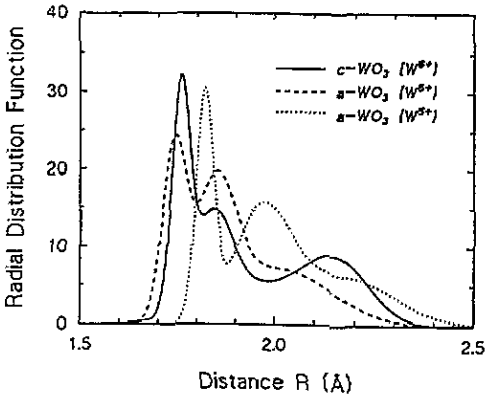

Figure 5. Radial distribution functions for the first coordination shell of tungsten in monoclinic crystalline c-WO_3 and a-WO_3 thin films around W^{6+} and W^{5+} sites derived from the four-component best-fit procedure.

Let us notice that, in spite of the possibility of describing the experimental EXAFS in the one- or two-component models, the total agreement between calculated signal and experiment is not good enough. To our knowledge, tungsten ions are octahedrally coordinated in c-WO_3, as in a-WO_3 [4, 14], and besides the distribution of the W–O distances is not continuous. There are several more-or-less well defined groups of distances which correspond to short terminal W=O groups, middle bridging W–O–W bonds and long non-bridging W–OH_2 bonds [3, 17]. The total EXAFS signal from the first shell is the sum of the contributions from distances in each group. Therefore, having this information, one can improve the agreement between the model and experiment by including more components

in the fitting procedure. It is important to note that such a step is physically justified due to *a priori* known structural information. The result of our best-fit analysis shows that the experimental EXAFS signal in the first shell cannot be adequately described by the three-component model, and an account of more than four components does not improve the agreement. The results of the four-component fit are presented in table 1 and figure 4(*b*). The estimated error bars for all parameters are shown in table 1 in brackets. We utilized in the fit the EXAFS formula in the harmonic approximation [4]; therefore to each of four components one can compare with a Gaussian distribution, so that the total radial distribution function (RDF) inside the first coordination shell can be reconstructed (see figure 5). It is necessary to stress that such information cannot be obtained at the present time by any other experimental technique, including x-ray diffraction, due to its weak sensitivity to the local environment.

From the obtained structural data (table 1) for the transparent and coloured a-WO_3 thin films and c-WO_3, one can see that in all cases there are three groups of distances that are well observed in RDF (figure 5) as three peaks of differing height and width. In crystalline c-WO_3, where tungsten atoms are formally in a 6+ valence state, the peaks are well defined even at large distances (~ 2.15 Å) and are split into two main groups: 1.7–2.0 Å and 2.0–2.4 Å. In amorphous thin films, the shape of the distribution differs essentially from the crystalline case: the longest bonds have greater Debye–Waller factor values, therefore the last peak is broadened and the centre of the distribution is shifted to a region of smaller distance. The position of the distribution for a-WO_3 depends strongly on the valence state of tungsten, and is shifted to longer distances for tungsten ions in a 5+ valence state. The average tungsten–oxygen distances, calculated as $\langle R \rangle = (\sum_i R_i N_i)/(\sum_i N_i)$, are equal to 1.928 Å (c-WO_3, XRD), 1.929 Å (c-WO_3), 1.881 Å (W^{6+} in a-WO_3) and 1.992 Å (W^{5+} in a-WO_3). Note that the agreement between the XRD and EXAFS data for c-WO_3 is very good. The difference between the bond lengths for W^{6+} and W^{5+} is equal to ~ 0.11 Å, i.e. about 6% of the W^{6+}–O distance. Such large changes in the average tungsten–oxygen distance means that the formation of W^{5+} ions leads to significant distortions of the lattice around them. The Debye–Waller factor correlates with the value of the tungsten–oxygen bond and increases when the last one increases. This result is in good agreement with known bond-length–bond-strength (valence) correlations for mixed-valence tungsten oxides [18].

Thus, the strong interaction between injected unpaired electrons trapped at tungsten sites and the lattice leads to a displacement of the oxygen around tungsten ions, reflecting the change of the bond lengths and the degree of [WO_6] octahedral distortion. Therefore, we conclude that the structural changes observed by x-ray absorption spectroscopy in a-WO_3 thin films under colouration correspond to the formation of small-radius polarons.

4. Summary and conclusions

In this paper we have presented a study of the local environment around tungsten ions in transparent and coloured a-WO_3 thin films by x-ray absorption spectroscopy. The analysis of the XANES and EXAFS parts of the experimental spectra confirms the hypothesis of the formation of small-radius polarons under thin-film colouration. This effect is accompanied by a strong lattice deformation around the tungsten ions with trapped electrons, and by the rearrangement of their electronic structure with the formation of W^{5+} ions.

Acknowledgments

JP and AK wish to thank the Laboratori Nazionali di Frascati for hospitality during their stay there. They are especially thankful to Professor E Burattini and to the staff of the PWA laboratory for the possibility of making measurements at the PWA BX-1 beam line EXAFS station.

References

[1] Granqvist C G 1992 *Solid State Ionics* **53–56** 479–89
[2] Kleperis J J, Cikmach P D and Lusis A R 1984 *Phys. Status Solidi a* **83** 291–7
[3] Daniel M F, Desbat B, Lassegues J C and Garie R 1988 *J. Solid State Chem.* **73** 127–39
[4] Balerna A, Bernieri E, Burattini E, Lusis A, Kuzmin A, Purans J and Cikmach P 1991 *Nucl. Instrum. Methods* A **308** 234–9, 240–2
[5] Temmink A, Anderson O, Bange K, Hantsche H and Yu X 1990 *Thin Solid Films* **192** 211–8
[6] Faughnan B W, Crandal R S and Heyman P M 1975 *RCA Rev.* **36** 177
[7] Schirmer O F, Wittwer V and Baur G 1977 *J. Electrochem. Soc.* **124** 749
[8] Deb K 1973 *Phil. Mag.* **27** 801
[9] Davazoglou D and Donnadieu A 1988 *Thin Solid Films* **164** 369–74
[10] Burattini E, Purans J and Kuzmin A 1993 *Japan. J. Appl. Phys.* (in press)
[11] Kuzmin A (unpublished)
[12] Kuzmin A, Purans J, Benfatto M and Natoli C R 1993 *Phys. Rev.* B **47** 2480–6
[13] Rehr J J, Mustre de Leon J, Zabinsky S I and Albers R C 1991 *J. Am. Chem. Soc.* **113** 5135–40
Mustre de Leon J, Rehr J J, Zabinsky S I and Albers R C 1991 *Phys. Rev.* B **44** 4146–56
[14] Loopstra B O, Boldrini P 1966 *Acta Cryst.* **21** 158–62
[15] Purans J, Kuzmin A and Burattini E 1993 *Japan. J. Appl. Phys.* (in press)
[16] Chaboy J, Garcia J, Marcelli A and Tyson T A 1993 *Japan. J. Appl. Phys.* (in press)
Chaboy J, Tyson T A and Marcelli A 1993 *Japan. J. Appl. Phys.* (in press)
[17] Balerna A, Bernieri E, Burattini E, Kuzmin A and Purans J 1990 *Proc. 2nd European Conf. on Progress in X-ray Synchrotron Radiation Research, Roma* **25** (Bologna: SIF) pp 679–82
[18] Domengès B, McGuire N K and O'Keeffe M 1985 *J. Solid State Chem.* **56** 94–100
Daniel M F, Desbat B, Lassegues J C, Gerand B and Figlarz M 1987 *J. Solid State Chem.* **67** 235–47